Numerical Simulation and Analysis of the Three-Step Excavation of an Extra-Large Cross-Section and a Low Flat-Ratio Railway Tunnel

Wenxing Huo
China University of Petroleum Huadong
Xue Shifeng (zhangp963598@163.com)
China University of Petroleum Huadong
Zongzhi Zhao
CCCC First Highway Engineering Group Co, Ltd
Zhiyu Gao
CCCC First Highway Engineering Group Co, Ltd
Mingyue Shao
CCCC First Highway Engineering Group Co, Ltd

Research Article

Keywords: extra-large section tunnel, three-step method, finite element analysis, middle pipe shed

Posted Date: March 31st, 2021

DOI: https://doi.org/10.21203/rs.3.rs-316940/v1

Numerical Simulation and Analysis of the Three-Step Excavation of an Extra-Large Cross-Section and a Low Flat-Ratio Railway Tunnel

Wenxing Huo[1,2], Shifeng Xue[1], Zongzhi Zhao[3] Zhiyu Gao[3], Mingyue Shao[3]

[1]*College of Pipeline and Civil Engineering, China University Of Petroleum (Huadong), Qingdao, 266580, China*

[2]*China Communications Construction Company Limited, Beijing, 100088, China*

[3]*CCCC First Highway Engineering Group Co,Ltd., Beijing, 100024, China*

Correspondence should be addressed to Xue Shifeng; E-mail: zhangp963598@163.com

Abstract: The Xinbaishiyan tunnel in the reconstruction Chengdu-Kunming railway Ermeishan-Mipan section mainly runs through dolomite with dolomitic limestone, with an excavation area of 260 m^2, a maximum span of 22.3 m, a maximum height of 14.4 m, a vector height of 7 m, and a rise-span ratio of 0.31. The tunnel has an extra-large cross-section and it is a low flat-ration railway tunnel. This paper mainly describes the the finite element analysis for this tunnel excavation that was used to guide the construction. Finite element software was used to model the tunnel according to the engineering geological conditions of the tunnel. These engineering geological conditions included the rock mass, system bolts, middle pipe shed, steel arch and shotcrete, grouting layer, second lining and so on. Nonlinear construction phase analysis was adopted. The results showed that the maximum vertical deformation of the tunnel vault and the middle of the invert was about 34 mm. The vertical deformation of the tunnel could be divided into an acceleration deformation section, linear deformation section, deceleration deformation section, and stable deformation section. The maximum horizontal deformation in the middle of the side wall was about 12.3 mm. Under the effect of the initial support, the equivalent stress of the side wall gradually increased with the excavation of the steps and the increase of the support structure. The axial force of the bolt in the middle of the side wall was larger than that in other places and the axial force of the middle pipe shed went along with the excavation of the tunnel in waves. The steel arch and the shotcrete had the maximum effective stress at the arch shoulder, which played the role of the deformation and pressure for the surrounding rock. During the construction, the length and height of the three-step method had to be set reasonably. The middle pipe shed and the system bolt supported the rock mass together. In the construction of the extra-large cross section and the flat tunnel, there was no need to set up temporary support, which was convenient for mechanical excavation.

Keywords: extra-large section tunnel, three-step method, finite element analysis, middle pipe shed

1. Introduction

The stability of surrounding rock is very important during tunnel construction. To ensure the stability of surrounding rock excavation, appropriate excavation methods should be selected according to the surrounding rock grade and water seepage. After selecting the construction methods based on engineering experience during large-span tunnel construction, the selected excavation methods should be analyzed to ensure the stability of the tunnel excavation.

The extra-large cross-section tunnels always include a tunnel with more settings in the import and export as station tunnels and a tunnel with surrounding rock breakage due to import and export and complicated geological conditions. This produces construction difficulty and the need to adopt a numerical simulation and field test the reliability of the tunnel construction. China has produced certain achievements in the study of such tunnels. Xi Jiami et al.[1] conducted a comparative study on the three-step excavation method and the double-side wall diversion pit method of a long-span tunnel and concluded that the double-side wall diversion pit method produced less ground settlement than the step-method and

that the double-side wall diversion pit method was safer than the step-method. Zhang Junru and Ou Xiaoqiang et al.[2] studied the demolition of the temporary support of a secondary lining. They pointed out the evolution of the safety factor in each stage of the demolition and support, and they pointed out that the reasonable length of the one-time demolition and support of the double side wall diversion pit method was about 9 m. Wang Weifu and Mei Zhu et al. [3] made a comparative analysis of the step method, the center cross diagram (CRD), and double side-wall drift pilot excavation, and they proposed the excavation method of a three-step temporary invert plus vertical support. The actual construction showed that this method was efficient and fast.

China has built several extra-large cross-section tunnels. The exit section of the Xinkaotang tunnel of the Ganlong railway, completed in 2014, is the third-line tunnel of "2 main lines + 1 tie line." The maximum excavation width of the tunnel is 30.26 m, the maximum height is 16.94 m, and the maximum excavation area exceeds 390 m^2. For the New Zhijiawan tunnel of the Yuxiang railway line II the largest span is 22 m and the largest excavated area is 250 m^2. The maximum excavation width of the Gongbei tunnel[4] of the Zhuhai connecting line of the Hong Kong-Zhuhai-Macao bridge is 19 m, the maximum height is 21 m, and the excavation area is 337 m^2. The Yingpan road tunnel[5] in Changsha city adopts advanced full-section pre-reinforcement, double-layer steel pre-support, and reasonably organized shallow excavation. The ultra-deep and large-section underwater tunnel was successfully excavated with a depth span ratio of only 0.46 and an area of 376 m^2, which overcame the difficulties of multi-process and multi-section in the construction of the ultra-large-section underwater tunnel. With the development of tunnel and underground space engineering, the amount of long-span tunnels is increasing.

The construction of a large-section tunnel generally adopts the method of step excavation, and the main construction methods are: step method, middle wall engineering method (center diagram method (CD), CRD), single side wall drift pilot method, double side-wall drift pilot excavation, cylinder hole method, wall hole method, etc. Its core principle is reliance on the auxiliary construction methods to translate a large section into a small cross section. The arch department is constructed first. Then the construction wall or wall arch construction occurs as soon as possible to have a better section tunnel closed loop. Then the excavation and inverted arch core soil occur, dismantling the temporary support. The conversion system forms the large cross section tunnel. The main construction problem is a complex process of cohesion that is unfavorable to mechanization construction. The temporary support is difficult to remove, and the system conversion time is long.

The tunnel studied in this research was the Xinbaishiyan tunnel in the Reconstruction Chengdu-Kunming railway Ermeishan-Mipan section. The tunnel has an excavation area of 260 m^2, a maximum span of 22.3 m, a maximum height of 14.4 m, a vector height of 7 m, and a rise-span ratio of 0.31. Because the three-step method was simpler than the double-wall guide pit method and mechanical excavation was available, there was no problem of system transformation caused by the removal of temporary supports. According to the engineering geological conditions of the Xinbaishi tunnel, the finite element method was used to analyze and study the three-step construction[6].

2. An engineering example

2.1. Project summary

The Xinbaishiyan tunnel in the reconstruction Chengdu-Kunming railway Ermeishan-Mipan section mainly runs through dolomite with dolomitic limestone, and the maximum depth is about 470 m. The lithology is mainly light gray, off-white middle thick block dolomite mixed with dolomitic limestone. Thin layers and bands of siliceous rocks are occasionally

encountered, the rock strata affected by faults are broken, and the overall stability is poor. The tunnel inlet side is around 1200 m for the three line tunnel station. The V level of the surrounding rock, rock trends, and oblique line was up to the angles of 45 ~56. The section of the tunnel is shown in Figure 1. The components include: C30 shotcrete, 350 mm thick, section steel HW300 × 300 × 10 × 15 arch frame, with a spacing of 1000 mm, middle pipe shed, adopting a Φ76 steel pipe wall thickness of 7 mm, 8 m long, 400 mm spacing, self-drilling bolt adopting a Φ28 steel tube wall thickness of 6 mm, 4 m long, according to a 1000 mm × 1000 mm arrangement, and C40 concrete lining thickness of about 900 mm.Groundwater types of bedrock fissure water, karst water, and covering layer pore water mainly occur in the dolomite and the fault fracture zone along the rock level and fault fracture zone to the next to the river discharge, narrow tunnel buried depth, and displacement for the tunnel construction. The finite element analysis did not consider the water.

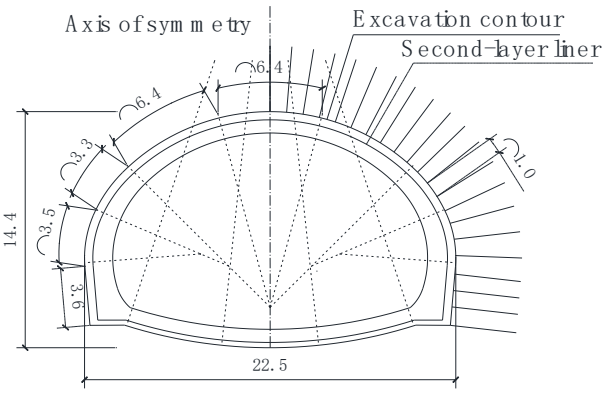

FIGURE 1: Tunnel section (m)

2.2. Brief description of three-step tunnel excavation

As shown in Figure 2, the three-step method was divided into three steps: the upper, middle, and lower steps and four parts of the invert. Each step was 5 m long and the distance from one step to the invert was 15 m. The construction process was: first the middle pipe shed was hit, then the upper step ① was excavated. After the upper excavation was completed, the initial support was applied for the upper hole body, namely the initial shotcrete.

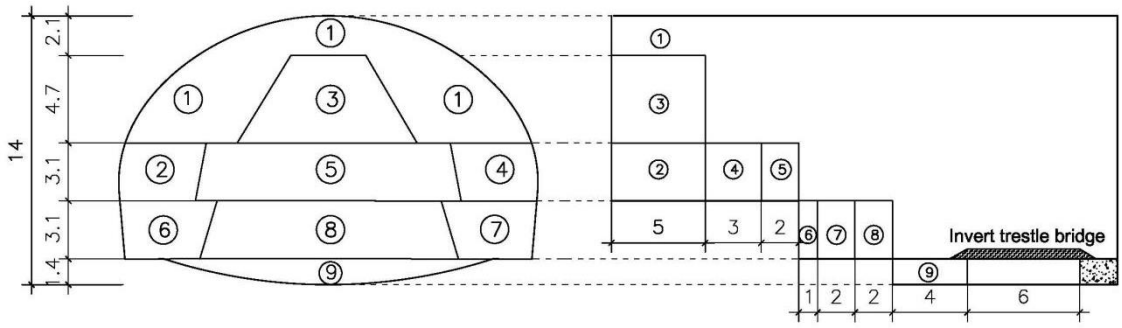

FIGURE 2: Three-step construction section view (m)

The steel arch was erected, and the rock bolt was hit. After the construction of the upper step reached 5 m, the left side ② of the middle step and the upper core soil ③ were excavated in order to provide the initial support for the step structure in the left side of the cave body with the same supporting structure ①. After ② construction to 1 m, the right part of the middle step was excavated in order to provide the initial support for the step structure in the right hole body. After ④, the construction to 3 m, excavation occurred ⑤ in the step of the core soil. After the ⑤ was excavated 1 m, excavation occurred in accordance with the ② and ④ construction methods for the lower steps ⑥ ⑦. Then the excavation of the lower step of the core soil ⑧, the upper, middle, and lower steps, retained a distance of 5 m. Finally, during the excavation

of invert ⑨, the support structure had to be closed. The support structure closure and invert excavation and support had to be carried out in time. The excavation footage had to be 1 m.

2. Numerical calculation

2.1 Elements types and yield criteria

2.1.1. Selection of the element types. Midas GTS NX finite element software was used for modeling and analysis. The surrounding rocks were assumed to be continuous interstitium. The shotcrete and the steel arch were simulated by the shell element with equal stiffness. The middle pipe shed was simulated by an implantable beam unit. The self-drilling bolt was simulated by an implantable truss element. The grouting layer and the second lining were simulated by the body element. The time-dependent creep of the surrounding rock was not considered, and the linear elastic constitutive model was adopted for the support system and the secondary lining.

2.1.2. Plastic yield criterion. The Mohr-Coulomb yield criterion was applied and the yield was based on the maximum shear stress. See Formula 1 for the yield function, where the range of the Lode angle was $0 \ll \theta \ll 60°$. The yield failure surface is shown in Figure 3.

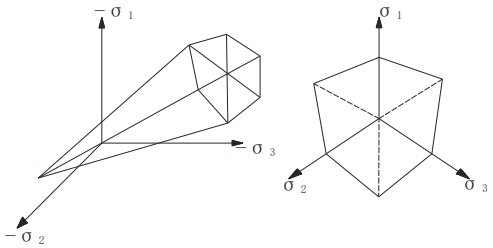

FIGURE 3 Mohr-Coulomb failure surface in the principal stress space

$$F(\underline{\sigma}) = \frac{\sin\phi}{3} I_1 + \sqrt{J_2}\left(\cos\theta - \frac{1}{\sqrt{3}}\sin\theta\sin\phi\right) - c\cos\phi = 0. \qquad (1)$$

In the formula, $I_1 = \sigma_x + \sigma_y + \sigma_z$ is the first invariant of the stress tensor, $J_2 = \frac{1}{6}\left[\left(\sigma_x - \sigma_y\right)^2 + \left(\sigma_y - \sigma_z\right)^2 + (\sigma_z - \sigma_x)^2\right] + \tau_{xy}^2 + \tau_{yz}^2 + \tau_{zx}^2$ is the second invariant of the stress tensor, $\theta = \frac{1}{3}\cos^{-1}\left(\frac{3\sqrt{3}}{2}\frac{J_3}{J_2^{3/2}}\right)$ is the Lode angle, that is, the angle between the first principal stress and the deviatoric stress components in the principal stress space, $J_3 = s_x s_y s_z + 2\tau_{xy}\tau_{yz}\tau_{zx} - s_x\tau_{yz}^2 - s_y\tau_{zx}^2 - s_z\tau_{xy}^2$ is the third invariant of the stress tensor, and $\left(s_x, s_y, s_z\right)$ is the stress deviation ($= \underline{\sigma} - \sigma_{mean}$).

2.1.3. Related flow law. According to Mises's plastic potential theory, the components of the plastic strain increment were determined by the differential of the plastic potential function to the stress components.

$$d\varepsilon_{ij}^p = d\lambda\frac{\partial g(\sigma_{ij})}{\partial\sigma_{ij}}. \qquad (2)$$

Or the matrix form

$$\{d\varepsilon^p\} = d\lambda\left\{\frac{\partial g(\sigma)}{\partial\sigma}\right\}. \qquad (3)$$

In the formula, $d\varepsilon_{ij}^p$ is plastic and should be an incremental tensor, $\partial g\left(\sigma_{ij}\right)$ is the stress tensor, and $d\lambda$ is the proportionality constant.

There were two kinds of flow rules: correlation and discorrelation. The plastic potential function was assumed to be

consistent with the failure function $g(\sigma_{ij}) = f'(\sigma_{ij})$ of the flow law. The fact that the failure surface and the plastic potential energy surface coincided was called the correlative flow law. The plastic strain increment $\delta\varepsilon_{ij}^{p}$ was orthogonal to the failure surface (plastic potential surface). All of the points of the initial stress σ_{ij}^{*} of the soil had be within the plastic potential surface.

2.1.4 Elastic-plastic stress-strain equation.

$$\{d\sigma\} = [D]d\{\varepsilon\} - [D]d\{\varepsilon^{P}\}. \quad (4)$$

According to the failure criterion, the relationship between plastic stress and strain was:

$$\left\{\frac{\partial f(\sigma)}{\partial \sigma}\right\}^{T}\{d\sigma\} = \frac{dF}{dH}\left\{\frac{\partial H}{\partial \varepsilon^{p}}\right\}^{T}\{d\varepsilon^{p}\}, \quad (5)$$

where $f(\sigma)$ is the failure function and $\mathrm{F} = f(H)$ is the function of the hardening parameter H.

Equation (4) was substituted into Equation (5), and the flow rule Equation (3) was substituted into equation (5) to obtain:

$$d\lambda = \frac{\left\{\frac{\partial f(\sigma)}{\partial \sigma}\right\}^{T}[D]d\{\varepsilon\}}{\left(\frac{dF}{dH}\left\{\frac{\partial H}{\partial \varepsilon^{p}}\right\}^{T} + \left\{\frac{\partial f(\sigma)}{\partial \sigma}\right\}^{T}[D]\right)\left\{\frac{\partial g(\sigma)}{\partial \sigma}\right\}}. \quad (6)$$

Equation (6) was substituted into Equation (3):

$$d\{\varepsilon^{P}\} = \frac{\left\{\frac{\partial g(\sigma)}{\partial \sigma}\right\}\left\{\frac{\partial f(\sigma)}{\partial \sigma}\right\}^{T}[D]}{\left(\frac{dF}{dH}\left\{\frac{\partial H}{\partial \varepsilon^{p}}\right\}^{T} + \left\{\frac{\partial f(\sigma)}{\partial \sigma}\right\}^{T}[D]\right)\left\{\frac{\partial g(\sigma)}{\partial \sigma}\right\}}d\{\varepsilon\}. \quad (7)$$

The corresponding relationship between the components of the plastic strain increment and the total strain component was given, and Equation (7) was substituted into Equation (4) to obtain:

$$(d\sigma) = \left([D] - \frac{\left\{\frac{\partial g(\sigma)}{\partial \sigma}\right\}\left\{\frac{\partial f(\sigma)}{\partial \sigma}\right\}^{T}[D]}{\left(\frac{dF}{dH}\left\{\frac{\partial H}{\partial \varepsilon^{p}}\right\}^{T} + \left\{\frac{\partial f(\sigma)}{\partial \sigma}\right\}^{T}[D]\right)\left\{\frac{\partial g(\sigma)}{\partial \sigma}\right\}}\right)d\{\varepsilon^{P}\}. \quad (8)$$

The solution method of the common nonlinear equation was adopted, and the convergence criterion was satisfied.

2.2. Model establishment

The rock parameters were selected according to the geological exploration data of the Xinbaishiyan tunnel in the reconstruction Chengdu-Kunming railway Ermeishan-Mipan section. The element material properties of the middle pipe shed, bolt support, steel arch, and shotcrete composite shell are shown in Table 1.

Tab.1 Material physical parameters

Material	Surrounding rock 1	Surrounding rock 2	Pipe shed	Tunnel bolt	Steel arch support with shotcrete	Grouting layer	The second line
Bulk density (kN/m^3)	23	26	78.5	78.5	24	20	25
Modulus of elasticity (GPa)	3.0	2.0	210	210	30	0.2	32.5
Poisson's ratio	0.3	0.35	0.3	0.3	0.2	0.3	0.3
Angle of internal friction（°）	46	27					
Cohesive force (Pa)	400	200					
The dilatancy Angle（°）	5	4					
Cross-sectional area			15174	414.7			

(mm^2)

The width boundary of the calculated model was selected to be four times the tunnel span, with the height boundary reaching 100 m at the top of the tunnel, the bottom boundary reaching 50 m at the bottom of the tunnel, and a span of 22.3 m. Therefore, the total length of the established model boundary was 142 m, the total height was 164.4 m, and the tunnel depth was 60 m. The boundary conditions of the calculation model were as follows: the bottom surface was the vertical constraint, the upper boundary was the free boundary, a vertical pressure of 1400 kPa was loaded, the left and right boundaries were the transverse constraint, and the front and rear boundaries were the longitudinal constraints. The finite element model is shown in Figure 4, and the supporting and excavation surface is shown in Figure 5, with 94417 elements in total.

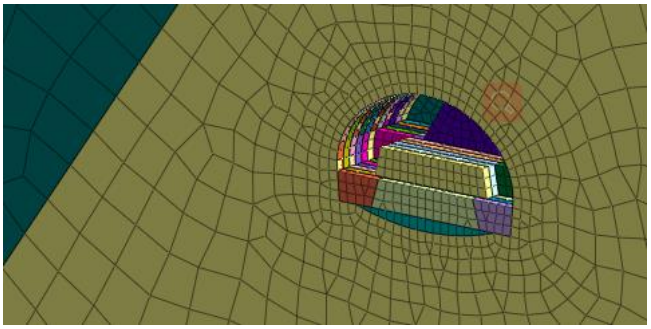

FIGURE 4 Tunnel model

2.3 Surrounding rock deformation analysis

The nonlinear construction stage analysis was applied to the model, which was divided into 49 construction stages, each of which was 1 m in depth. The tunnel support and excavation surface after 49 steps of excavation are shown in Figure 5, and the tunnel deformation results are shown in Figure 6. The soil excavation surface deformation trend was upward and the excavation of the lateral and maximum deformation occurred in the second step in the central core soil surface. The maximum deformation was 42 mm[7]. The upper tunnel deformation was down, the lower deformation was upward due to the large span, and the tunnel was under the load. The deformation of the excavation face during the early supporting small, and the left side of the excavation face had far greater deformation. The early stage of the two lining concrete inverted arch deformations was small.

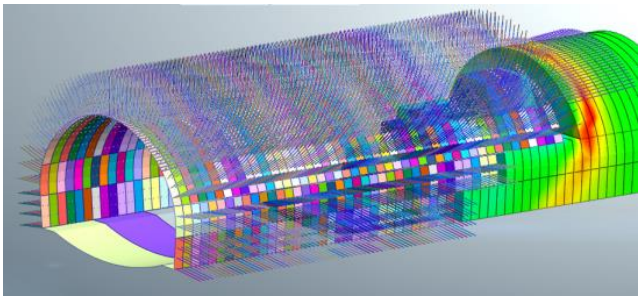

FIGURE 5 Tunnel support structure

2.3.1. Vertical deformation. The vertical deformation cloud diagram of the tunnel after the 49th excavation step is shown in Figure 7. The maximum settlement at the vault was 34.2 mm, and the upward deformation in the middle of the invert was 34.0 mm.

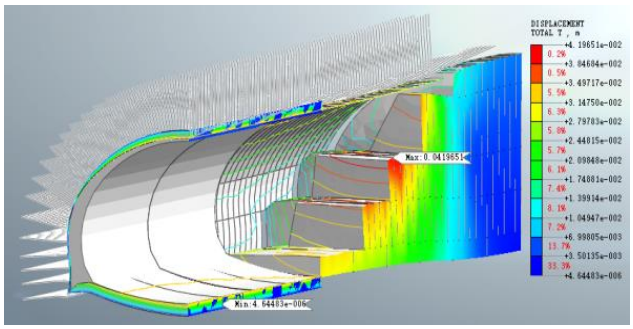

FIGURE 6 Deformation map of the tunnel and the excavation face

In the process of the excavation of the tunnel, all of the parts of the initial excavation face of the tunnel settled down with the excavation step, as shown in Figure 8. The vault in the tunnel had an excavation length of 15 m before the settling velocity was larger. For 15 m to 40 m, the excavation subsidence speed was slow. At 40 m and 50 m, there was settlement stabilization in the excavation. The excavation face was about two times the hole diameter measuring point distance, there was deformation stability, and the maximum subsidence value was 33.63 mm.

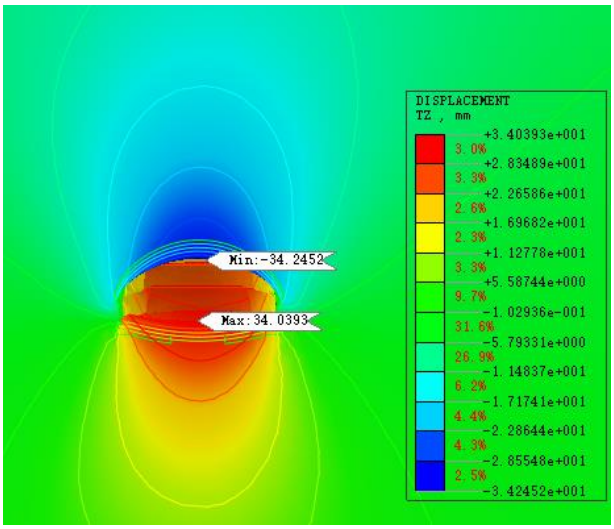

FIGURE 7 The tunnel deformed vertically after the excavation in step 49

The soil mass of the invert ⑨ was excavated at Step 25, but the middle part of the invert was rapidly raised with the excavation of the upper core soil ③ and the uplift tended to be stable at the 25 m elevation. When excavated at 50 m, the maximum uplift value was 34.04 mm. The settlement of the other parts was relatively small and the settlement increased with the increase of the excavation length. In the fourth position, the volume of the uplift gradually decreased with the excavation of the lower step ⑥ in the Step 14.

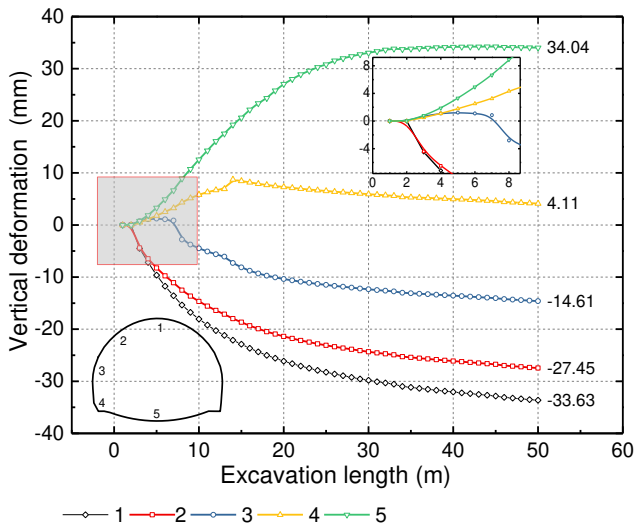

FIGURE 8 Each part of the initial excavation face settled down with the excavation step

The vertical deformation of the tunnel vault every 5 m along the length of the tunnel with the tunnel excavation step is shown in Figure 9. The settlement value of the soil body before excavation gradually increased with the approach of the excavation face, and the settlement speed was small. The settlement value of the arch soil directly above the excavation face increased rapidly with the increase of the excavation footage. Since the excavation face was further away, the settlement value tended to be stable, and the settlement point of each part gradually tended towards consistency. see Figure

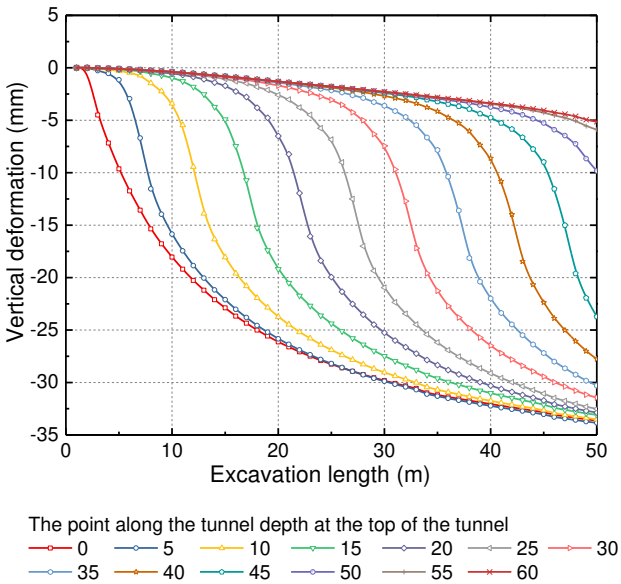

FIGURE 9 Vertical deformation of the tunnel vault with the excavation step

8 for Step 50 in the lower right corner. This step could be divided into the accelerated deformation section, linear deformation section, deceleration deformation section, and stable deformation section [8].

2.3.2. Horizontal deformation. The horizontal deformation of the tunnel at the 49th excavation step is shown in Figure 10. Due to the rock mass inclination during soil modeling, the horizontal deformation was not symmetrical.

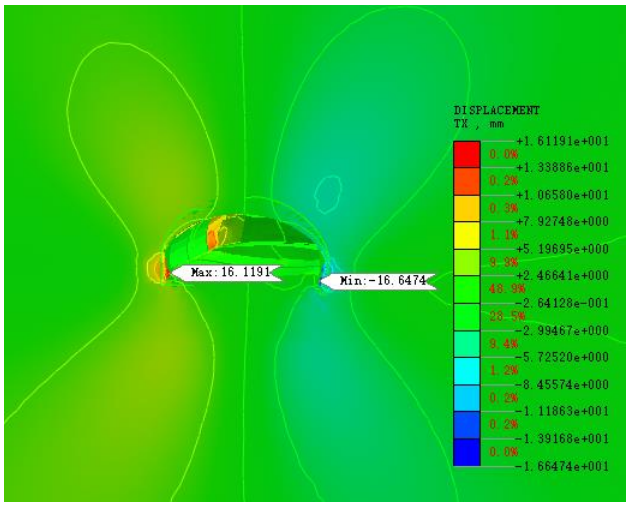

FIGURE 10 Horizontal deformation at Step 49 of the tunnel excavation

All of the parts of the initial excavation face horizontal deformation with the excavation steps In the process of excavation of the tunnel are shown in Figure 8. The deformation was the largest in three parts. The maximum deformation value increased with the excavation step. To the left ② of Step 7, the slope of the deformation increased after excavation. To the lower step left ⑥ of Step 13, the slope of the deformation increased rapidly after excavation, to the maximum value of 12.28 mm in Step 33. Finally, the deformation converged to 12.07 mm. Position 2 was at the top of the middle step, and the slope of the deformation increased rapidly after the excavation to the left ② of Step 7 and to the lower step left ② of Step 12. At position 4, the slope of the deformation increased slightly after excavation and the maximum value was 4.50 mm at Step 33. Position 1 had a smooth curve compared with other parts, and the maximum value was 3.07 mm at Step 33. Combined with the analysis of the excavation steps, the deformation increased with adjacent soil excavation. The second lining was applied in Step 34, and the deformation of each part decreased slightly after reaching the maximum value in Step 33. After the vertical deformation of the second lining, it was extruded to both sides, so there was a reaction to the horizontal deformation of both sides.

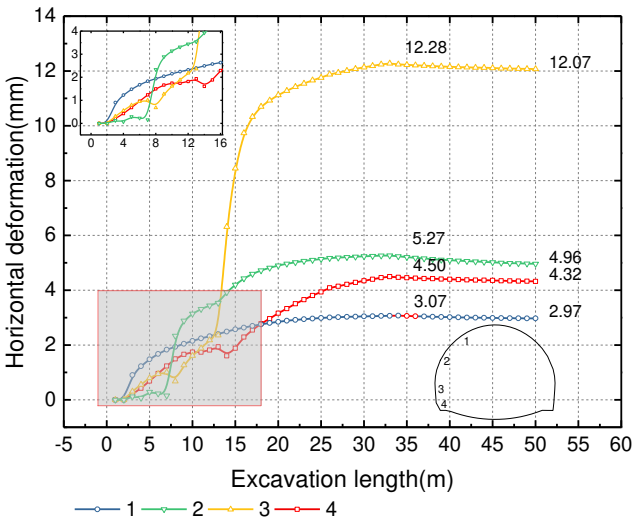

FIGURE 11 Each part of the initial excavation face deformed horizontally with the excavation step

The central tunnel side wall was located down the lower steps to the left of side ⑥. The horizontal deformation every 5 m along the depth of the tunnel with the excavation step is shown in Figure 12. With the upper step ① excavation the deformation increased, and with the middle step ② excavation the deformation was gentle, increasing slowly until the

lower step left ⑥ excavation of the deformation slope increased rapidly. After three steps, the deformation tended to be smooth. The final deformation was concentrated in the range of 11~13 mm.

There were two stationary segments in the deformation curve. The first stable stage was caused by the extrusion effect of the left side of the step on the middle of the tunnel side wall, and the deformation in the middle of the side wall stagnated during the excavation of the middle step, indicating that the lower step played a protective role in the rock mass of the side wall. With the excavation of the soil in the middle of the lower step of the side wall, the horizontal deformation of the side wall increased rapidly and finally tended to be stable. After the construction of the second lining, the horizontal deformation of the tunnel was reduced and the horizontal deformation of the part without the second lining was greater than that of the adjacent part with the second lining. The second lining had a greater inhibition on the horizontal deformation of the tunnel rock mass.

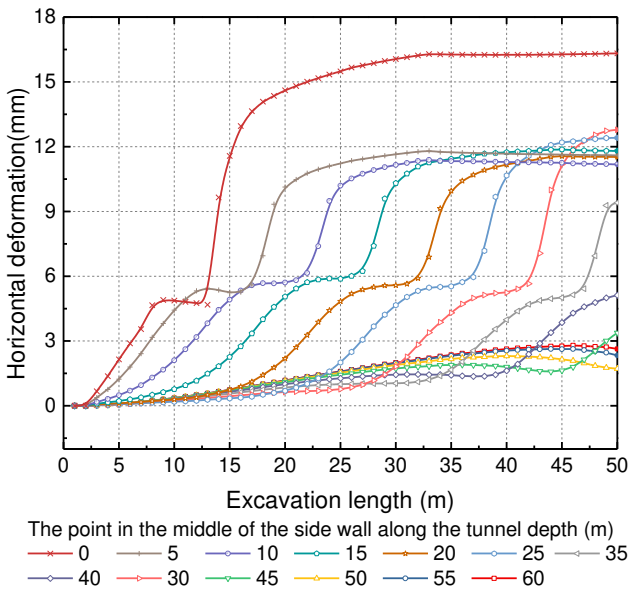

FIGURE 12 Horizontal deformation of the middle side wall with each excavation step

2.4. Surrounding rock stress analysis

2.4.1. Equivalent stress analysis. The equivalent stress distribution of the surrounding rock is shown in Figure 13. Under the action of the support structure, the effective stress at a certain distance from the lateral side wall reached the maximum value of 5.67 MPa. The effective stress on both sides of the invert was relatively large, about 4.0 MPa. The stress of the soil at the back of the excavation surface was about 4.0 MPa. Due to the effect of the middle pipe shed, the support of the excavated soil at the excavation surface was transferred to the soil at the back of the excavation surface, resulting in an increase in the stress of the soil at the back.

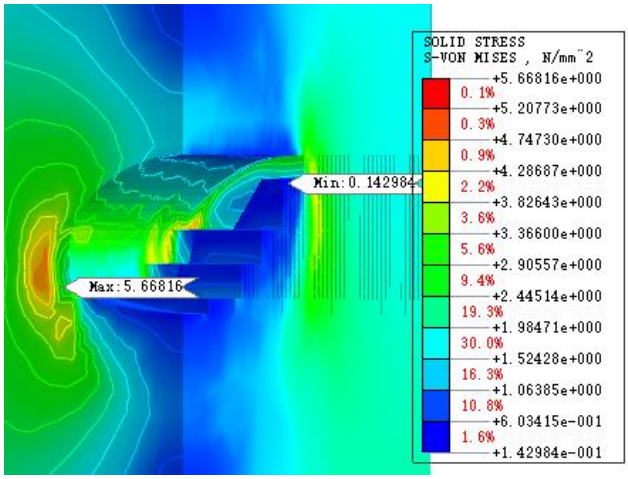

FIGURE 13 Equivalent stress nephogram

As shown in Figure 14, the equivalent stress changed for each part of the initial tunnel excavation face with the length of tunnel excavation. At Position 4, the equivalent stress increased gradually with the excavation of the tunnel. After the excavation of the first cycle invert, the stress growth curve tended to be smooth, and the maximum equivalent stress was 5.65 MPa. The effective stress at Arches 1 and 6 in the middle of the invert was released with the tunnel excavation, and this stress was lower than the initial effective stress. With the arch foot support after the excavation of the upper step ①, Position 3 increased sharply when the excavation reached 3 m. However, when the excavation stress was rapidly released on the left side of the middle step ②, the stress slightly increased with the excavation of the left side of the lower step ⑥. The change trend of Position 5 was the same as that of Position 4. When the increase of the tunnel excavation stress gradual increased, the maximum value was 2.93 MPa. After stress release, the stress of Position 2 increased slightly and tended to be gentle. With the increase of the excavation of the steps and the support structure, the equivalent stress changed with the transformation of the stress system. The gravity of the arch roof was transferred to both sides of the tunnel with the initial support, and the equivalent stress in the middle of the tunnel side wall increased gradually. During construction, the arch legs of the arch frame had to be firmly supported, and the bolts with locking legs had to be arranged.

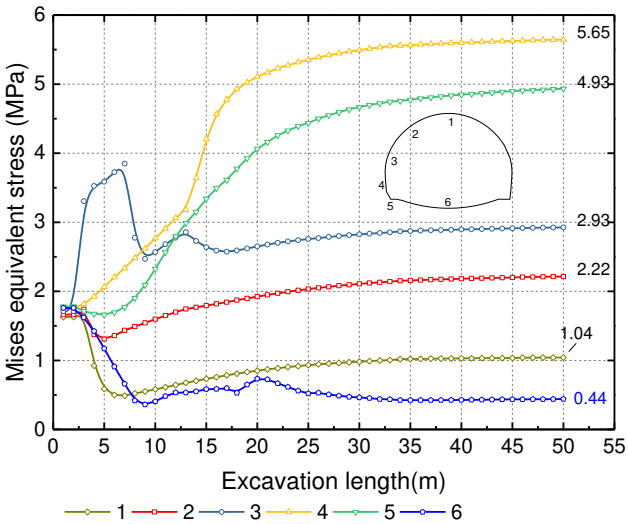

FIGURE 14 Diagram of the equivalent stress variation at each part of the tunnel with each excavation step

2.4.2. Primary stress analysis. Because the tunnel was relatively flat, under the action of the initial support structure, the main tensile stress appeared to have a positive value (about 0.07 MPa) at some parts of the tunnel vault, on both sides, and

in the middle of the invert, while no tensile stress appeared on the side wall, as shown in Figure 15.

The main tensile stress of each part of the tunnel increased with the excavation of the tunnel. The increase trend of the horizontal deformation at Position 3 was similar to the horizontal deformation shown in Figure 11. With the excavation of the left part of each step, a stagnation state appeared for Positions 1, 2, and 3. With the excavation of the tunnel, the main tensile stress first increased rapidly and then decreased slightly with the initial support gradually closed and without any tensile stress. Tensile stress appeared at Positions 4 and 5, with a maximum value of 0.07 MPa. With the second lining, the tensile stress gradually reduced to compressive stress, as shown in Figure 16. Due to the lack of a smooth arch, the tunnel invert and the foot of the arch were prone to failure due to tensile stress. High attention had to be paid to the construction, which had be closed early with a precocious ring.

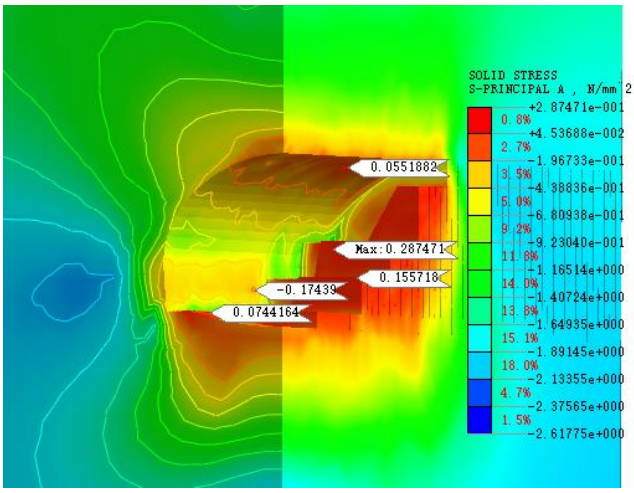

FIGURE 15 The first main response force

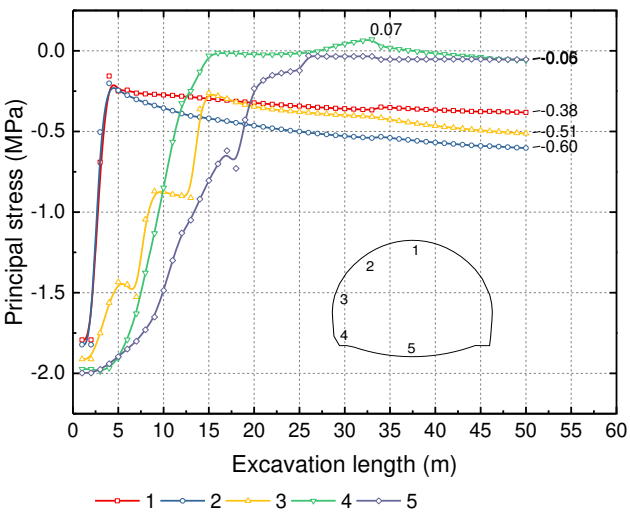

FIGURE 16 Diagram of the main tensile stress variation at each part of the tunnel along with the excavation step

2.4.3. Plastic zone analysis. The plastic zone development zone is shown in Figure 17. The color red represents the plastic zone formed by the single disturbance, blue represents the plastic zone formed by the secondary disturbance, and green represents the plastic zone formed by tensile stress. In Step 15, the plastic zone of the secondary disturbance appeared on the top and core soil, and the plastic zone of the single disturbance appeared on both sides of the invert. In Step 25, the plastic zone formed by tensile stress appeared at the location where the invert met the side wall. In Step 30, the plastic zone generated by the bottom tensile stress disappeared due to the secondary lining. The plastic zone at the bottom of the side

wall was large, and the plastic zone of the tensile stress appeared. The pressure transferred to this zone by the Initial support of the tunnel was large, and the surrounding rock was vulnerable to disturbance. Therefore, support had to be provided at the bottom of the side wall and on both sides of the invert during construction.

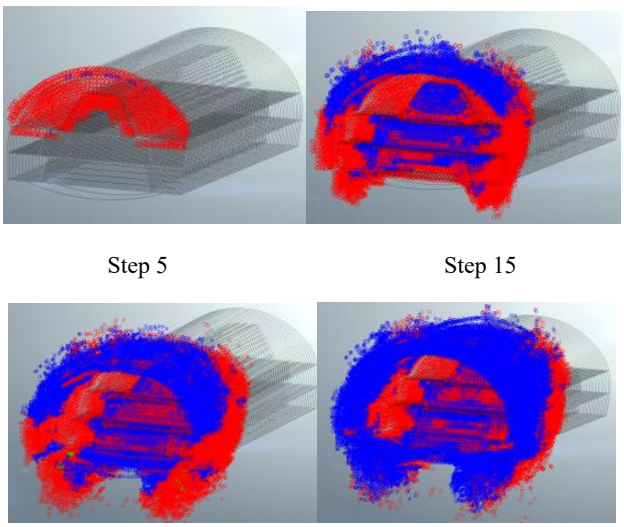

FIGURE 17 Pattern of the plastic development zone

2.5. Stress analysis of the initial support.

2.5.1. Middle pipe shed. As the tunnel was excavated, the vertical deformation of the pipe shed gradually increased and tended to be stable, with a maximum deformation of about 30 mm. Since the tail of the pipe shed in the front section of the tunnel was located below the front of the pipe shed in the rear section, and because there were superimposed parts in the front and rear middle sections, the vertical deformation of the front of the pipe shed in the rear section was slightly reduced. The bending moment of the pipe shed at the face of the tunnel was the largest, and the maximum value (0.23 kNm) was about three times the maximum value at other locations. The bending resistance of the pipe shed bought time for the bolting and shotcrete support of the steel arch frame erected after tunnel excavation. A representative middle pipe shed steel pipe 13 m from the initial excavation surface was selected in order to extract its axial force, as shown in Figure 18. With the excavation of the tunnel, the variation of the axial force of the pipe shed was complicated. When the excavation face was at the end of the pipe shed, the axial force of the pipe shed was as shown in excavation Step 13. The front end of the pipe shed was pulled and the tail was compressed. As the excavation face moved to the middle of the pipe shed, the pipe shed was in the middle of the axial pressure, and the front tension reached a maximum at the same time. The excavation Step 17 of the pipe shed steel tube axial force was carried out, the excavation face continued to move forward, and the pressure peak of the pipe shed moved forward[9]. When the excavation face reached the front of the pipe shed, the pipe shed was under overall axial pressure and the front-end pressure was greater than the end. Since the excavation face was far away from the front end of the pipe shed, the axial force at the back end of the pipe shed experienced little change, the pressure at the front end decreased, and the tension state was gradually restored. In the process of excavation, the axial force of the pipe shed changed in a complicated but regular way, The axial force changed in a wave shape[10] with the tunnel excavation step. After the excavation surface left the pipe shed, the change in the axial force of the pipe shed became smaller and smaller as the distance increased. The stress on the front and rear pipe sheds was continuous, and the deformation at the joints was coordinated[11].

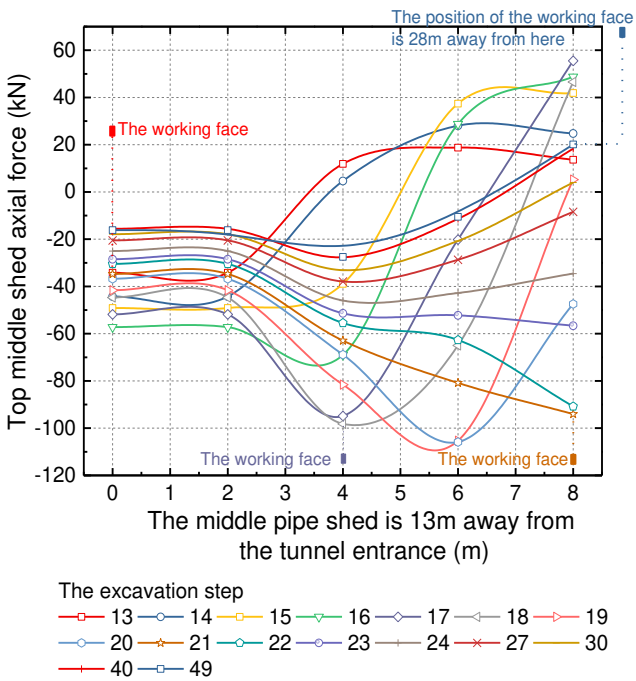

FIGURE 18 Axial force change diagram of the top pipe shed with the excavation steps

2.5.2. Tunnel bolt. The axial force of the bolt at Step 15 generally increased with the excavation of the tunnel, as shown in Figure 19. The axial force at the end of the arch roof bolt was slightly lower than the middle, the tail of the bolt at the bottom of the side wall was greater than that at the front, and the axial force of the other bolts was greater than that at the end. The axial force of the bolt bolt tended to be stable with the excavation of the tunnel. The maximum axial force of the bolt rod in the middle of the side wall was about 90 kN. The maximum axial force of the bolt rod at the foot of the arch of the upper step was 70 kN. The maximum axial force of the bolt rod at the vault was 40 kN, and the maximum axial force of the bolt rod at the bottom of the side wall was 19 kN. With the large horizontal deformation and equivalent stress in the middle of the side wall, the corresponding rock bolt axial force was also large[12]. When the rock mass in the middle of the side wall was excavated, the protection had to be strengthened. Since the rock bolt axial force increased gradually with the excavation step, the supporting effect became stronger and stronger.

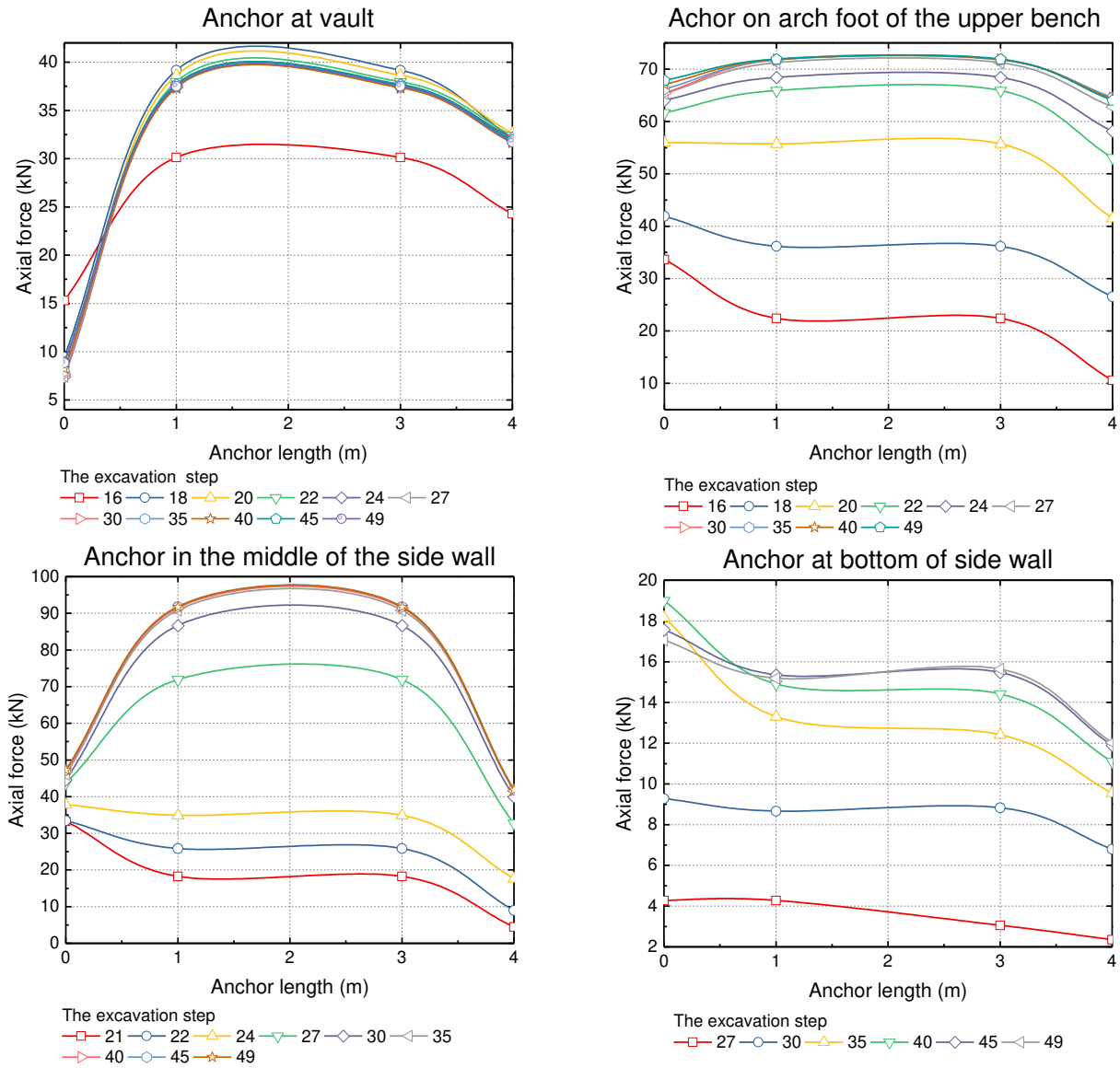

FIGURE 19 Variation diagram of axial force of rock bolt in different parts of tunnel with excavation step

2.5.3. Composite shell of the shotcrete and steel arch. The steel arch and the shotcrete in the initial support were converted into a single material according to the principle of equivalent compressive stiffness.[13]

$$E_0 = \frac{E_s A_s + E_c A_c}{A_0}. \qquad (9)$$

In the formula, E_c, E_s, and E_0 represent the sprayed concrete, steel arch shelf, and equivalent modulus of elasticity. A_a, A_s, and A_0 represent the section areas of the shotcrete and the steel arch as well as the total area of the section

It can be seen from the analysis results that the equivalent stress of the shell at the arch shoulder reached the maximum value of 27.4 MPa, as shown in Figure 20, and the bending moments of the vault and side wall were larger.

With the excavation of the tunnel, the annular compressive stress, equivalent stress, and circumferential bending moment of the shell generally increased, as shown in Figure 21. After the middle step excavation, the Position 3 stress increase rate was obvious. The pressure increased, the bending moment remained essentially stable, and the gravity of the vault was transferred to the middle of the side wall through the initial support. The stress of the shotcrete at the bottom of the invert was much less than that of other parts, and the stress was smaller.

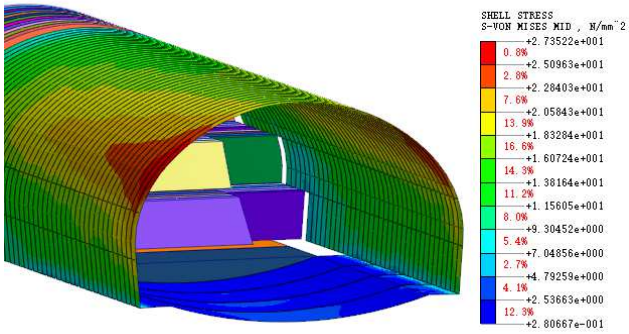

FIGURE 20 Equivalent stress cloud diagram of the composite shell

In the process of tunnel excavation, the steel arch and the shotcrete formed a closed-loop structure that played a role in transferring and redistributing the surrounding rock stress, and the timely erection of the steel arch and the shotcrete played a good role in the surrounding rock support.

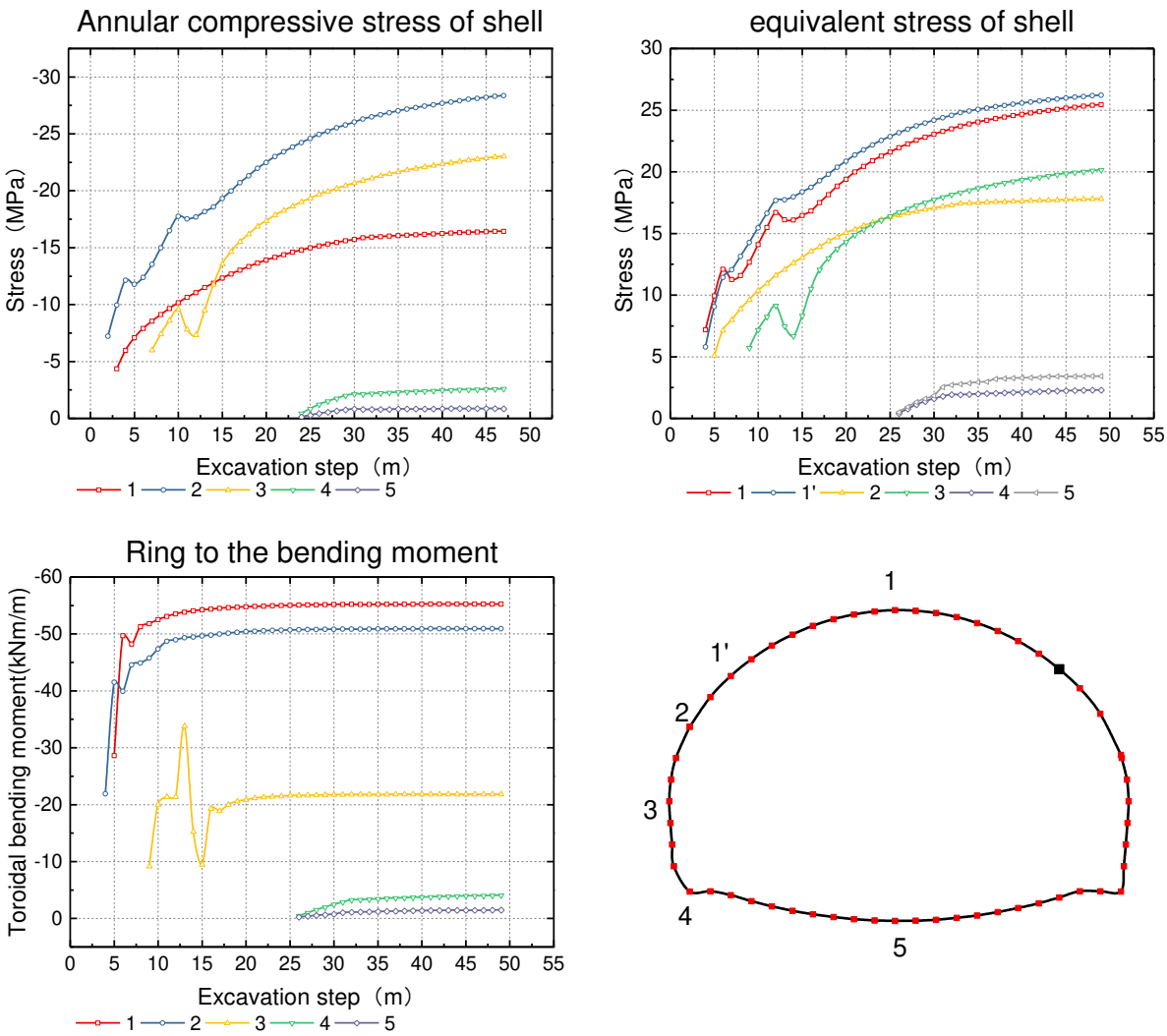

FIGURE 21 Changes of the annular compressive stress, equivalent stress, and annular bending moment of the composite shell with the excavation steps

3. Conclusions

The three-step method was not necessary to set up temporary support and there was convenient mechanical excavation, which was a great advantage. The middle pipe shed, system bolt, steel arch frame and shotcrete joint support rock mass were set up, and the three-step method's step length and step height were set reasonably to stabilize the excavation surface. The following conclusions were drawn through the finite element analysis.

(1) The vertical deformation of the arch roof and the arch bottom was relatively large, reaching 34 mm. According to the analysis in this study, the vertical deformation could be divided into four sections: The accelerated deformation section, linear deformation section, deceleration deformation section, and stable deformation section. The point that was about twice the diameter of the excavation edge made the vertical deformation tend to be stable. The horizontal deformation was the largest in the middle of the side wall, reaching 12.28 mm. With the excavation of the soil on the lower steps in the middle of the side wall. the horizontal deformation of the side wall increased rapidly and finally became stable, indicating that the lower steps excavated after the excavation played a protective role on the side wall. The horizontal deformation of the tunnel at the position of the second lining decreased slightly. Under the vertical pressure of the surrounding rock, the middle of the second lining of the side wall would extrude to the rock and soil.

(2) With the increase of the excavation of the steps and the support structure, the equivalent stress of the rock mass changed with the transformation of the stress system. The gravity of the arch roof was transferred to both sides of the tunnel with the initial support, and the equivalent stress in the middle of the side wall of the tunnel gradually increased. During the construction, the arch legs needed to be firmly supported, and bolts with locking feet had to be arranged. Pressure was transferred to the inverted arch and the foot of the tunnel through the Initial support, the surrounding rocks of which were susceptible to disturbance. At the same time, due to the failure of the tunnel section to form a smooth arch at the inverted arch position, tensile stress occurred in some construction stages. Rock and soil damage could easily occur, and the support at the bottom of the side wall and on both sides of the invert had to be done well in the construction. It was thus advisable to close the ring early.

(3) During the process of excavation, the axial force of the pipe shed changed in a complex and regular manner. Since the axial force of pipe shed changed in a waveform with the tunnel excavation, the change of the axial force of the pipe shed became smaller and smaller with the increase of the distance after the excavation surface left the pipe shed. The front and rear pipe sheds were under continuous stress and the joint deformation was coordinated.

(4) The horizontal deformation and the equivalent stress in the middle of the side wall were large and the corresponding axial force of the bolt was large. The protection in the middle of the side wall had to be strengthened. As the axial force of rock bolt increased gradually with the excavation steps, the supporting effect became stronger and stronger.

(5) The steel arch and shotcrete formed a closed-loop structure in the process of tunnel excavation, which played a role in transferring and redistributing the surrounding rock stress, and the timely erection of the steel arch and shotcrete played a good role in supporting the surrounding rock.

Declarations

Funding

No funding is received.

Conflicts of interests

The authors declare that they have no conflicts of interest.

Availability of data and material

The data in this paper include calculation result data and Finite element analysis data. All the data used to support the findings of this study are included within the article. There are not any restrictions on data access.

Code availability

Not Applicable.

Authors' Contributions

W. X Huo, S. F. Xue, Z. Z Zhao, Z. Y. Gao and M. Y. Shao have all participated in the designing framework, collecting data, analysis and interpretation of data, drafting, reviewing and approving the manuscript.

References

[1] XI Jia-mi，WANG Ming-ming，XU Feng， et al, "Num-erical simulation of construction method for shallow buri-ed large section tunnel,"Journal of Xi' an University of Science and Technology,vol.35,no.5 pp. 602-610,2015.

[2] ZHANG Junru,OU Xiaoqiang,Zheng Qiang,et al, "Study on the safety of large section tunnel under double layer initial su pport,"Modern Tunnelling Technology,vol.55,no.6 pp. 108-116 2018.

[3] WANG Weifu,MEI Zhu,"Study of Application of Bench Method to Shallow-buried Asymmetrically-pressured Railway Tunn el of Super-large Cross-section," Tunnel Construction,vol.37,no.12,pp. 1578-1584,2017.

[4] Villy A. Kontogianni and Stathis C. Stiros, "Induced deformation during tunnel excavation: Evidence from geodetic monito ring", Engineering Geology,vol.79,no.1-2,pp.115-126,2015.

[5] Chenghua Shi and Chengyong Cao and Mingfeng Lei, "Construction technology for a shallow-buried underwater interchang e tunnel with a large span," Tunnelling and Underground Space Technology, vol.70,pp.317-329,2017.

[6] Øyvind Dammyr,Bjørn Nilsen,Johannes Gollegger, "Feasibility of tunnel boring through weakness zones in deep Norwegian subsea tunnels," Tunnelling and Underground Space Technology,vol.69,pp.133-146,2017.

[7] Yuan Zhou, Yuming Zhu, Shumao Wang, Hu Wang,and Zhengxing Wang, "Rotational Failure Mechanism for Face Stability of Circular Shield Tunnels in Frictional Soils," Advances in Civil Engineering, Volume 2019, Article ID 7167802, 14 pa ges,2019.

[8] Zuo Qingjun,WU Youyin,YAN Tianxi, "Analysis of Time-space Effect for Surrounding Rock Deformation in Super-large C ross Section Slate Tunnel During Construction Period," Journal of Disaster Prevention and Mitigation Engineering,vol.38,no. 2,pp.233-243,2018

[9] Geng Daxin,Shi Yufeng, Yang Junsheng,Yang Feng, "Research on forepoling force of long and large pipe roof for shallow tunnel large section under existing highway," J.Huazhong Univ.of Sci.& Tech.(Natural Science Edition),vol.44,no.6,2016.

[10] Ki-Il Song,Gye-Chun Cho,Seok-Bue Chang,In-Mo Lee, "Beam–spring structural analysis for the design of a tunnel pre-rei nforcement support system," International Journal of Rock Mechanics and Mining Sciences,vol.59,pp.139-150,2013.

[11] Lan Jiang, Kejian Ma, Huagang Zhang, Qin Wu, Hongna Lu, and Qizhu Yang, "Seismic Behavior of Shear Connectors o f Steel Vierendeel Sandwich Plate," Mathematical Problems in Engineering, vol. 2019, Article ID 8047393, 14 pages, 201 9.

[12] HUO Wenxing, YUAN Bo, WANG Feng, JIANG Lan, "Succesive collapse resistance analysis of steel framework mounte d viscous dampers," WORLD EARTHQUAKE ENGINEERING, Vol.28, No.4, pp.111-115, 2012.

[13] J.P. Janin, D. Dias, F. Emeriault, R. Kastner, H. Le Bissonnais ,A. Guilloux,"Numerical back-analysis of the southern Tou lon tunnel measurements: A comparison of 3D and 2D approaches,"Engineering Geology,vol.195,pp.42-52,2015.

Figures

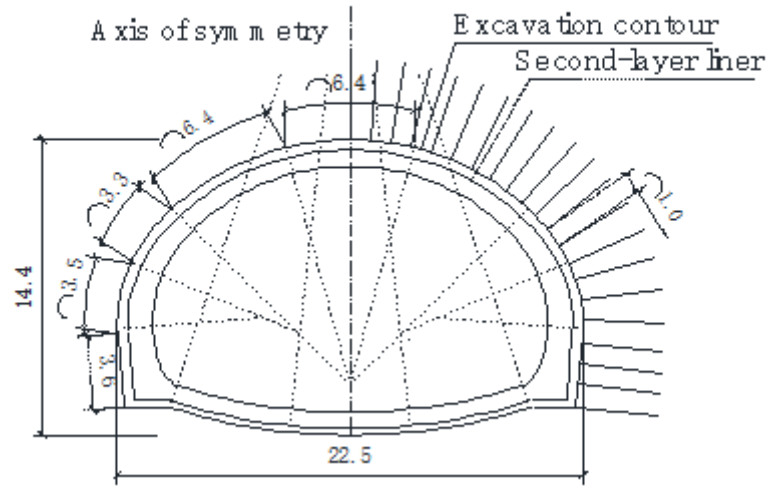

Figure 1

Tunnel section (m)

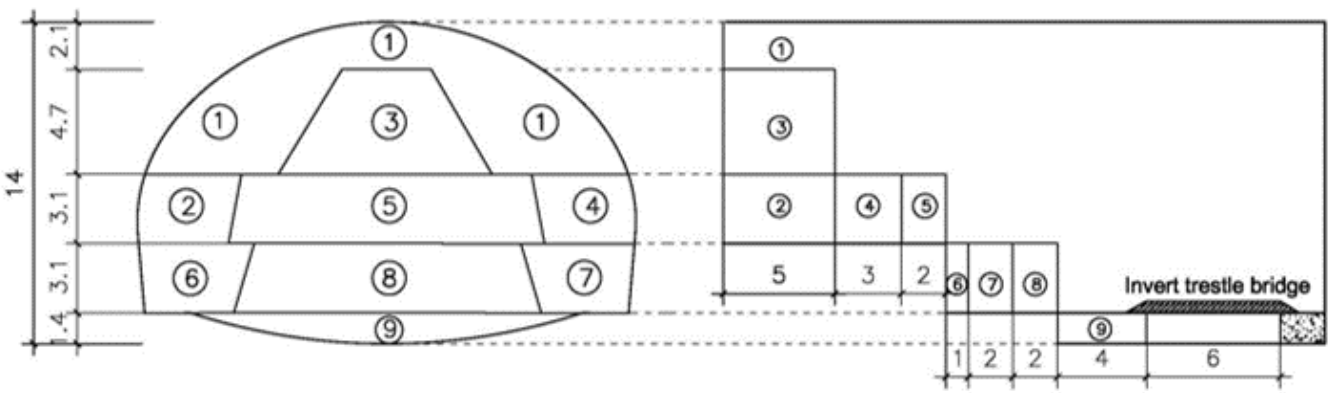

Figure 2

Three-step construction section view (m)

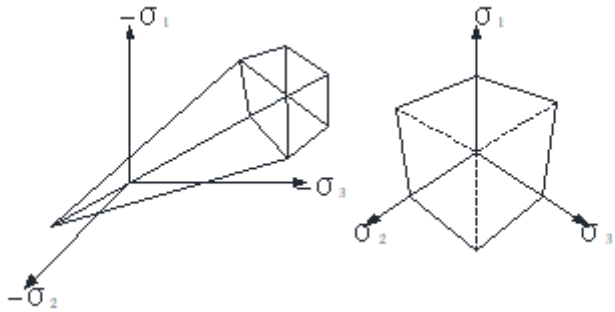

Figure 3

Mohr-Coulomb failure surface in the principal stress space

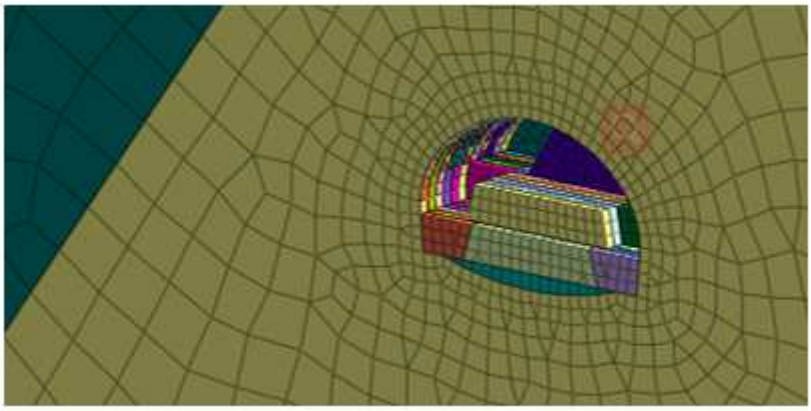

Figure 4

Tunnel model

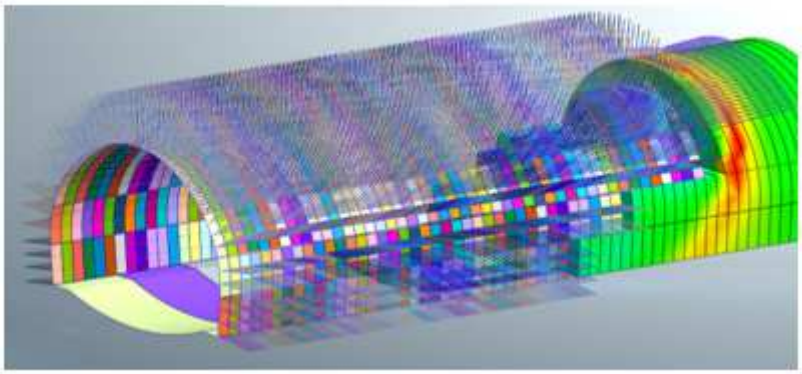

Figure 5

Tunnel support structure

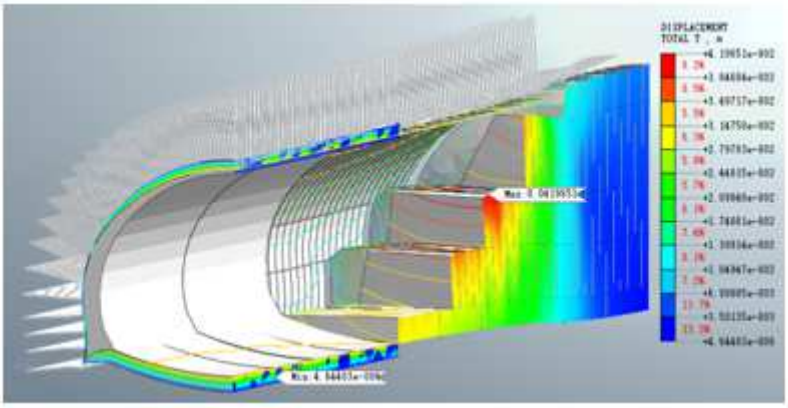

Figure 6

Deformation map of the tunnel and the excavation face

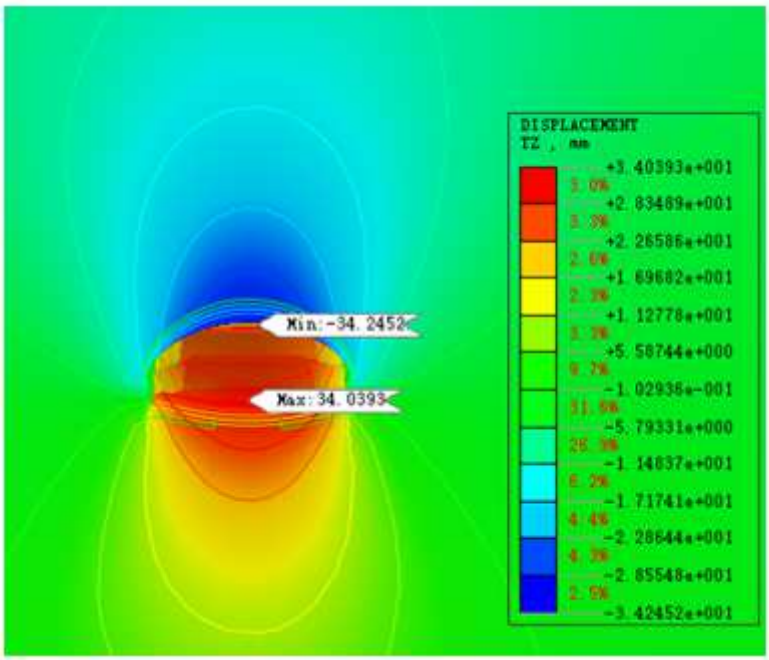

Figure 7

The tunnel deformed vertically after the excavation in step 49

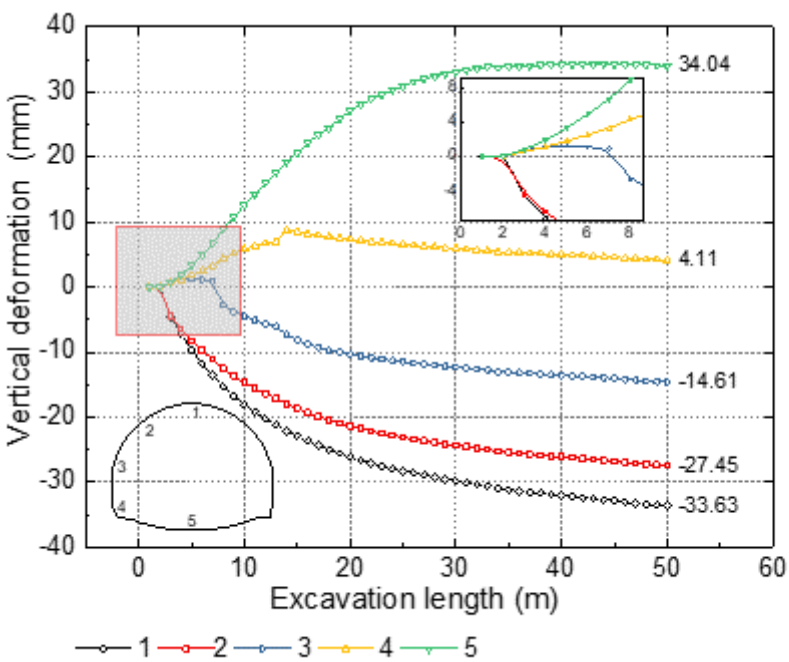

Figure 8

Each part of the initial excavation face settled down with the excavation step

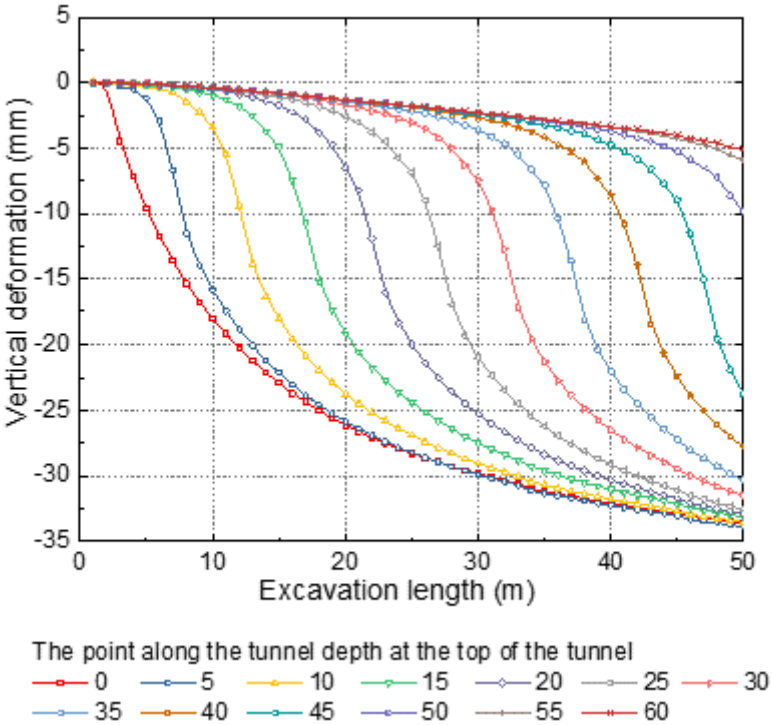

Figure 9

Vertical deformation of the tunnel vault with the excavation step

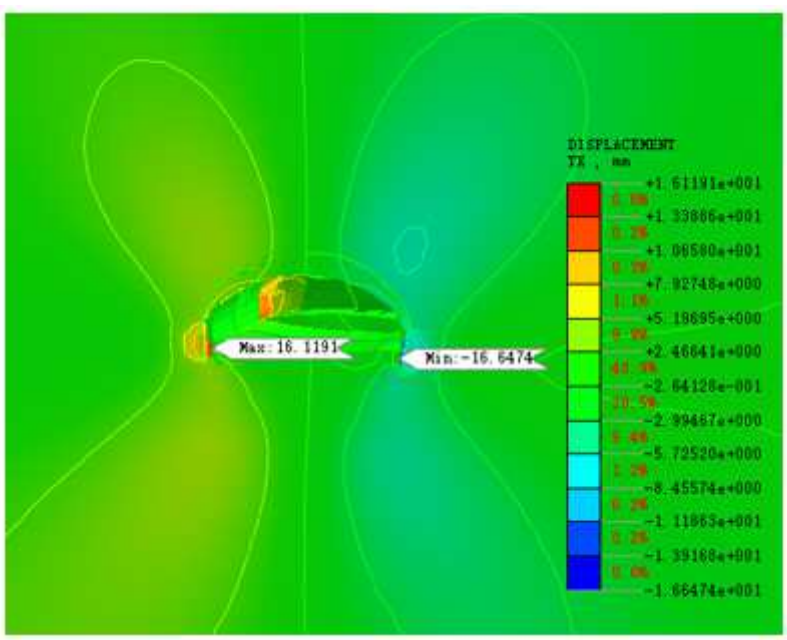

Figure 10

Horizontal deformation at Step 49 of the tunnel excavation

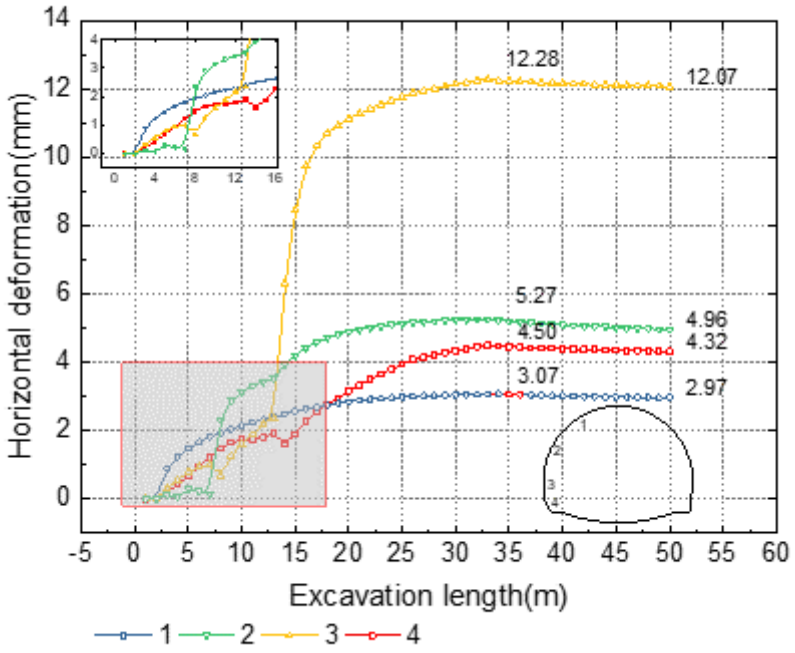

Figure 11

Each part of the initial excavation face deformed horizontally with the excavation step

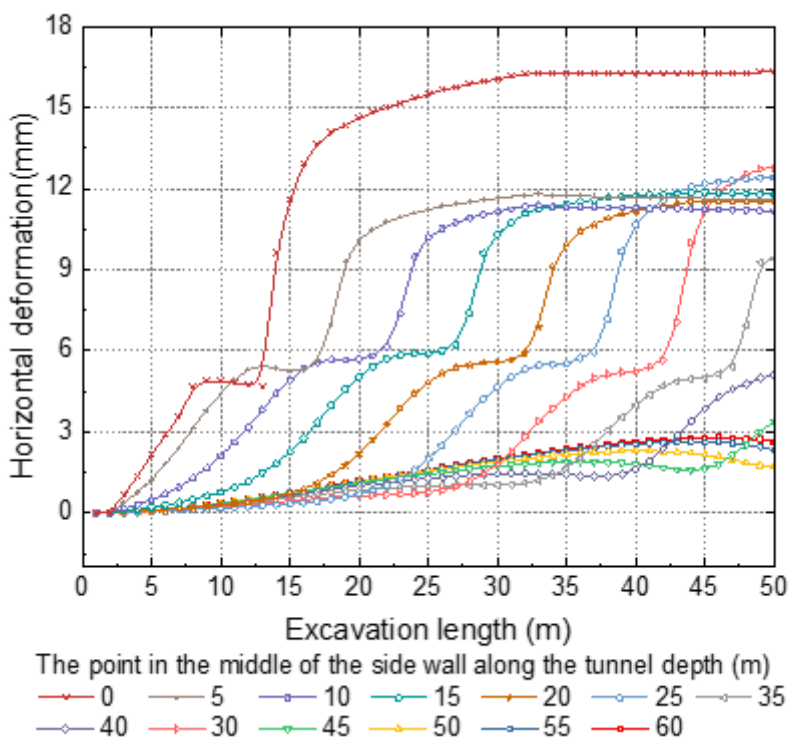

Figure 12

Horizontal deformation of the middle side wall with each excavation step

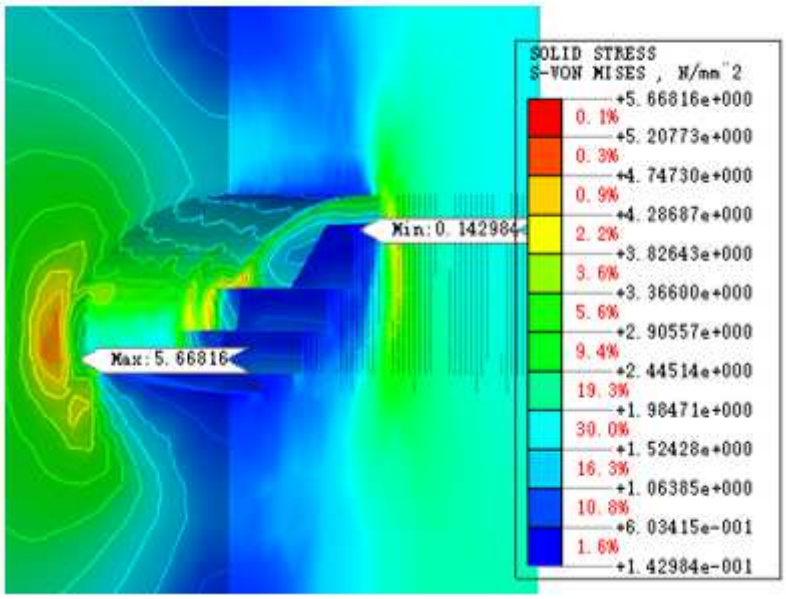

Figure 13

Equivalent stress nephogram

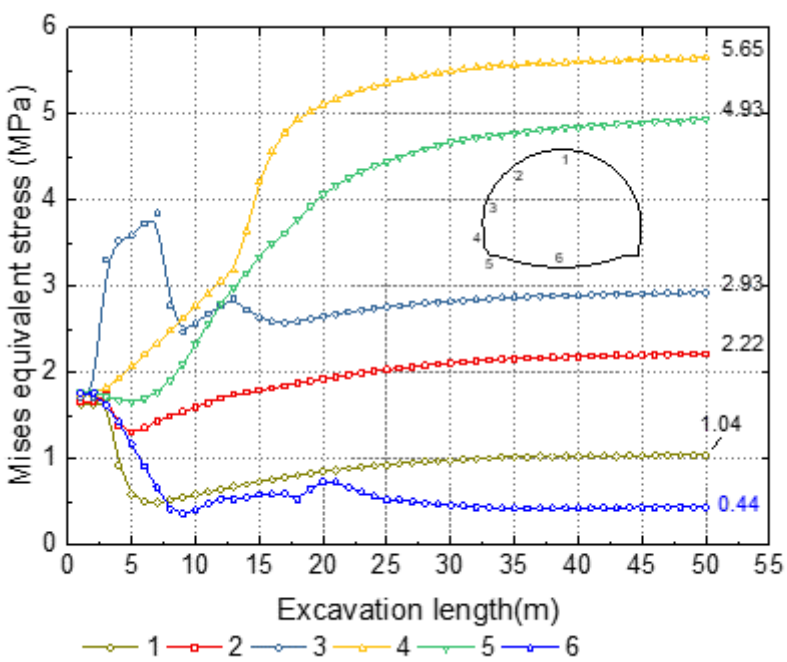

Figure 14

Diagram of the equivalent stress variation at each part of the tunnel with each excavation step

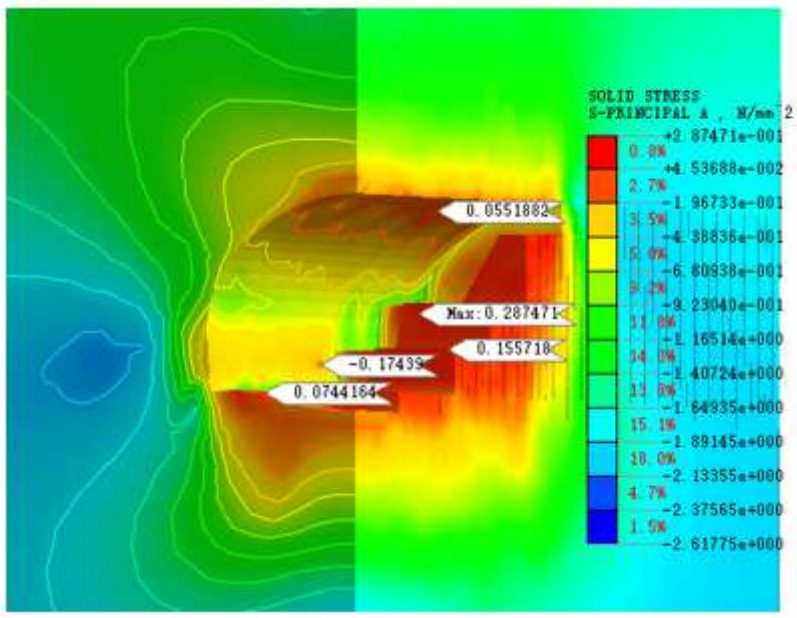

Figure 15

The first main response force

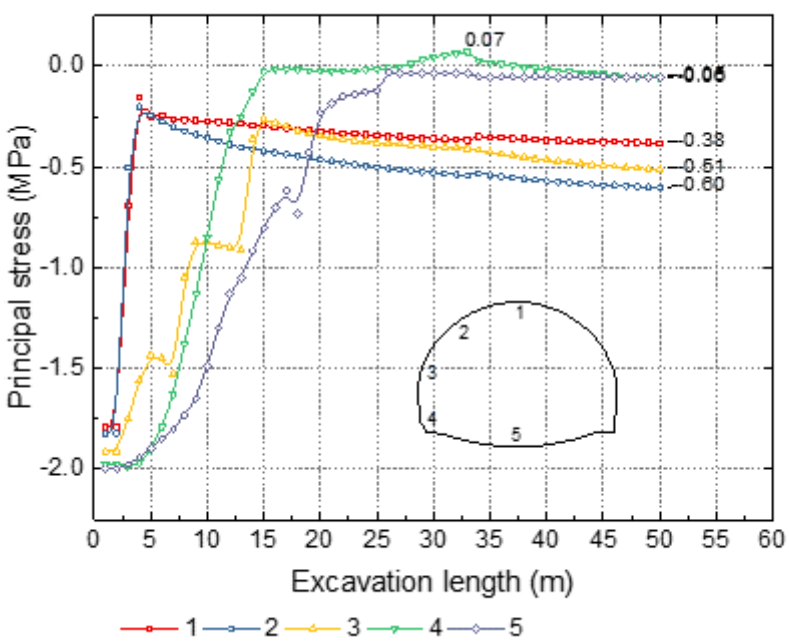

Figure 16

Diagram of the main tensile stress variation at each part of the tunnel along with the excavation step

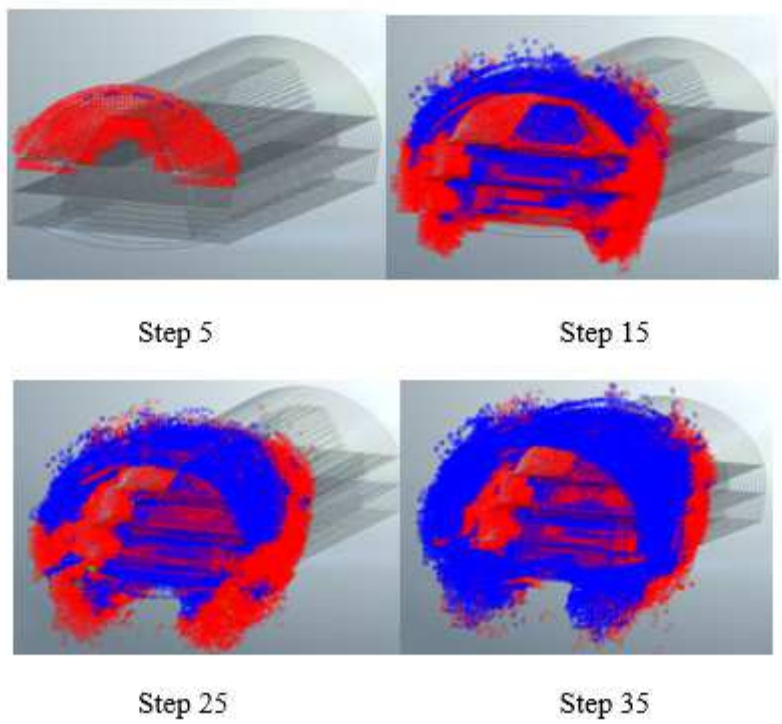

Figure 17

Pattern of the plastic development zone

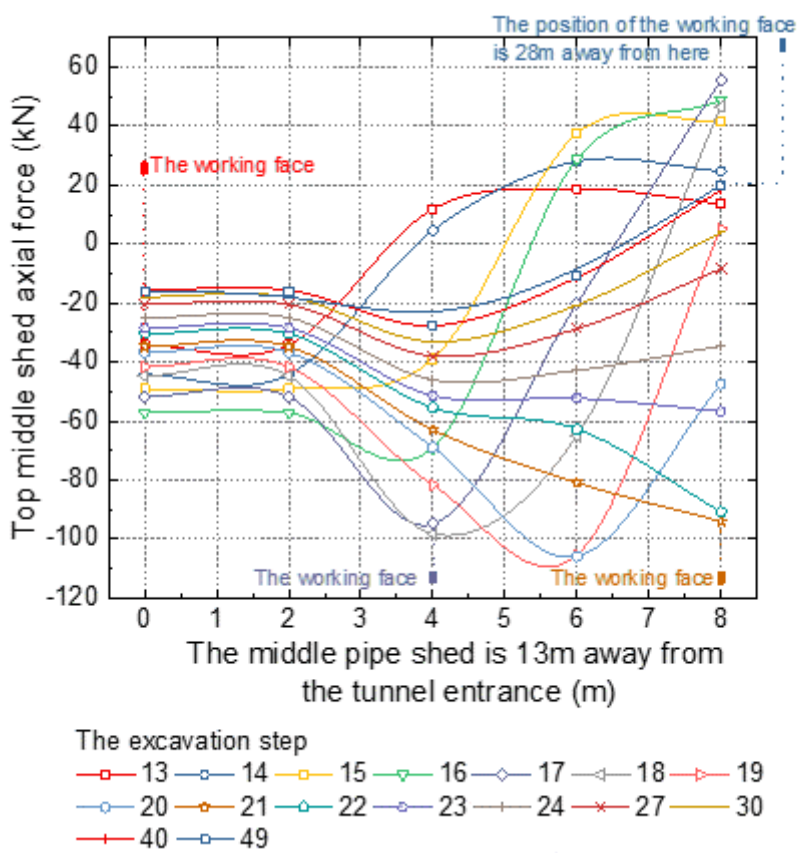

Figure 18

Axial force change diagram of the top pipe shed with the excavation steps

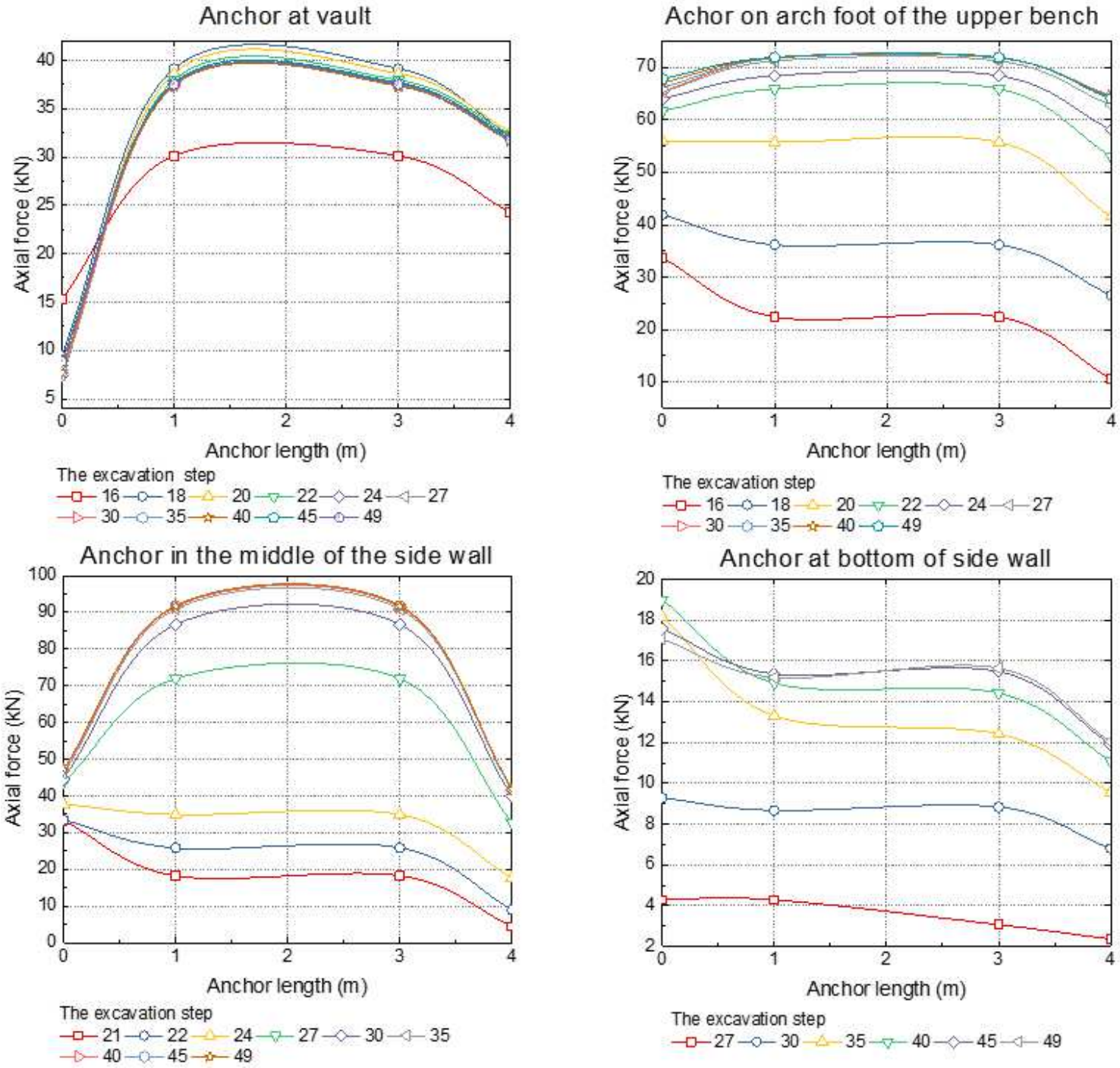

Figure 19

Variation diagram of axial force of rock bolt in different parts of tunnel with excavation step

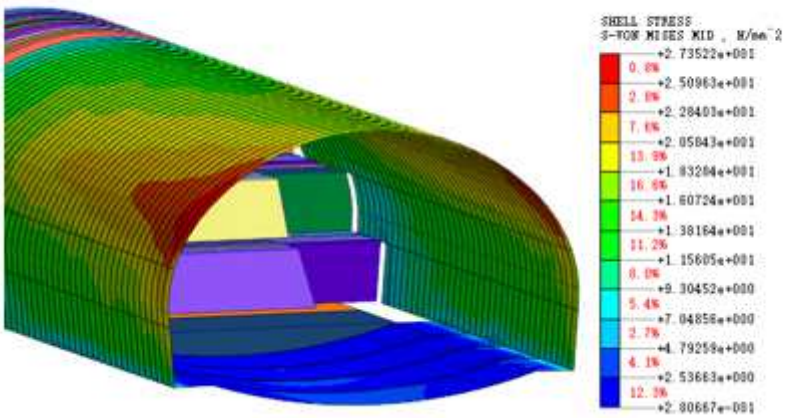

Figure 20

Equivalent stress cloud diagram of the composite shell

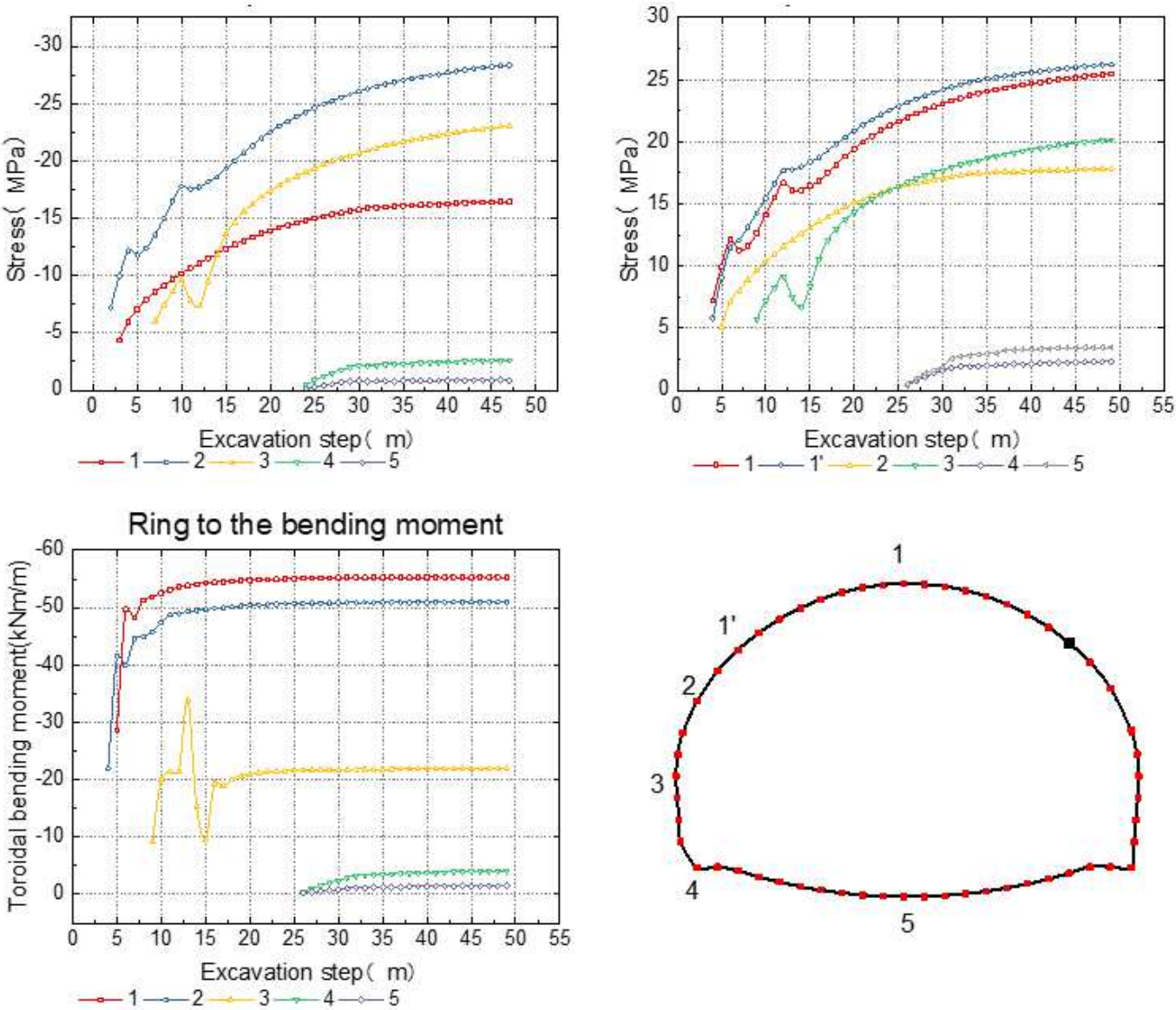

Figure 21

Changes of the annular compressive stress, equivalent stress, and annular bending moment of the composite shell with the excavation steps